Rational Design of New Conjugated Polymers with Main Chain Chirality for Efficient Optoelectronic Devices: Carbo[6]Helicene and Indacenodithiophene Copolymers as Model Compounds

Clément Gédéon, Natalia del Rio, Francesco Furlan, Andrea Taddeucci, Nicolas Vanthuyne, Vasilis G Gregoriou, Matthew John Fuchter, Giuliano Siligardi, Nicola Gasparini, Jeanne Crassous, et al.

Rational Design of New Conjugated Polymers with Main Chain Chirality for Efficient Optoelectronic Devices: Carbo[6]helicene and Indacenodithiophene Copolymers as Model Compounds

Clement Gedeon,[1,2,#] Natalia Del Rio,[2,#] Francesco Furlan,[3] Andrea Taddeucci,[4,5] Nicolas Vanthuyne,[6] Vasilis G. Gregoriou,[1,7] Matthew J. Fuchter,[3] Giuliano Siligardi,[4] Nicola Gasparini,[3,] Jeanne Crassous[2,] Christos L. Chochos[1,7*]*

[1] C. Gedeon, Dr. V. G. Gregoriou, Dr. C. L. Chochos, Advent Technologies SA., Stadiou Str, Platani 26504, Patras, Greece, E-mail: cchochos@advent.energy

[2] C. Gedeon, Dr. N. Del Rio, Dr. J. Crassous, Univ Rennes, CNRS, ISCR − UMR 6226, 35000 Rennes, France, E-mail: jeanne.crassous@univ-rennes.fr

[3] F. Furlan, Prof. M. J. Fuchter, Dr. N. Gasparini, Molecular Sciences Research Hub, Department of Chemistry, White City Campus, Imperial College London, 82 Wood Lane, London W12 0BZ, U.K.

[4] A. Taddeucci, Dr. G. Siligardi, Diamond Light Source, Harwell Science and Innovation Campus, Didcot, Oxfordshire, UK.

[5] A. Taddeucci, Dipartimento di Chimica e Chimica Industriale, University of Pisa, Via Moruzzi 13, 56124 Pisa, Italy.

[6] Dr. N. Vanthuyne, Aix Marseille University, CNRS, Centrale Marseille, iSm2, Marseille, France.

[7] Dr. V. G. Gregoriou, Dr. C. L. Chochos, Institute of Chemical Biology National Hellenic Research Foundation, Athens 11635, Greece.

# Contributed equally

Keywords: π-conjugated polymers, chirality, helicene, organic solar cells, self-assembly

Abstract

The unique properties of conjugated polymers (CPs) in various optoelectronic applications are mainly attributed to their different self-assembly processes and superstructures. Various methods have been utilized to tune and control CP structure and properties with less attention paid to the use of chirality. CPs with main chain chirality are rare and their microscopic and macroscopic properties are still unknown. In this work, we provide the first experimental results along these lines by synthesizing a series of racemic and enantiopure CPs containing statistical and alternating carbo[6]helicene and indacenodithiophene moieties and evaluating their microscopic (optical, energy levels) and macroscopic properties (hole mobilities, photovoltaic

performance). We demonstrate that a small statistical insertion of either the racemic or enantiopure helicene into the polymer backbone finely tunes the microscopic and macroscopic properties as a function of the statistical content. The microscopic properties of the enantiopure *vs.* the racemic polymers with the same helicene loading remain similar. On the contrary, the macroscopic properties, and more interestingly those between the two enantiomeric forms, are altered as a function of the statistical content. Once incorporated into a solar cell device, these chiral CPs display better performance in their enantiopure *vs.* racemic forms.

1. Introduction

Conjugated polymers (CPs) are seen as excellent candidate materials for the ever expanding applications of opto(bio)electronics, such as in organic light-emitting diodes (OLEDs), thin-film transistors (OFETs), organic photovoltaic cells (OPVs), organic photodetectors (OPDs) and organic electrochemical transistors (OECTs).[1] Bespoke synthesis of CPs allows tailoring of their chemical, electronic, and processing properties while identifying significant structure-to-property correlations. Over the past half century chemists have focused on synthesizing more complex and solution processable CPs, while advancing structural precision. These efforts have aimed to maximize their fundamental properties such as high charge carrier mobilities, tunable absorption and emission, as well as the ability to stabilize charges, among others. Yet, harnessing the full potential of CPs in organic electronics is incomplete and new (synthetic) design approaches are needed to provide the next generation of CP structures.

While chirality is ubiquitous in nature (polysaccharides, proteins, and nucleic acids), it has not yet been fully exploited in artificial soft materials, including CPs. Up to now, reports on chiral CP materials have mainly relied on the incorporation of either chiral side-chains, or the use of a chiral inducer, to generate thin films with strong chiroptical activity.[2] The applications of chiral CPs include asymmetric catalysis,[3] chiral separation,[4] chiral detection,[5] or chiral conductive polymers,[6] circularly polarized electroluminescent emitters for CP-OLEDs,[7] efficient spin filters via the chiral-induced spin selectivity (CISS effect),[8] magneto-optical materials,[9] and photodetectors.[2h-j] Despite such broad ranging applications, only a handful of CPs possessing chirality through enantiopure organic building blocks in the main chain polymer backbone have been synthesized, adequately characterized and incorporated into optoelectronic devices. This prevents the in-depth understanding of their photophysical properties, microstructures and device performance towards the design of next generation efficient chiral CPs.[7]

In this context, a judicious choice of chiral building block for the preparation of main chain chiral CPs may be the use of helicenes,[10] since they are fully π-conjugated helical molecules that possess semi-conducting activity and good chiroptical properties, such as strong electronic circular dichroism (ECD) and circularly polarized luminescence (CPL).[10, 11] However, in comparison to small molecule chiral materials, very few helicene-based enantioenriched CPs have been reported, [12] and only three of them contain carbo[6]helicene moieties (Figure 1).[12b,d,e] Furthermore, these previously reported polymers possess low molecular weights, closer to small oligomers[13]. Due to the rigid structure of the helicene core, the corresponding polymers (oligomers) exhibit low solubility in common organic solvents which limits their processability for the preparation of high-quality thin films, hindering the fabrication of efficient electronic devices.

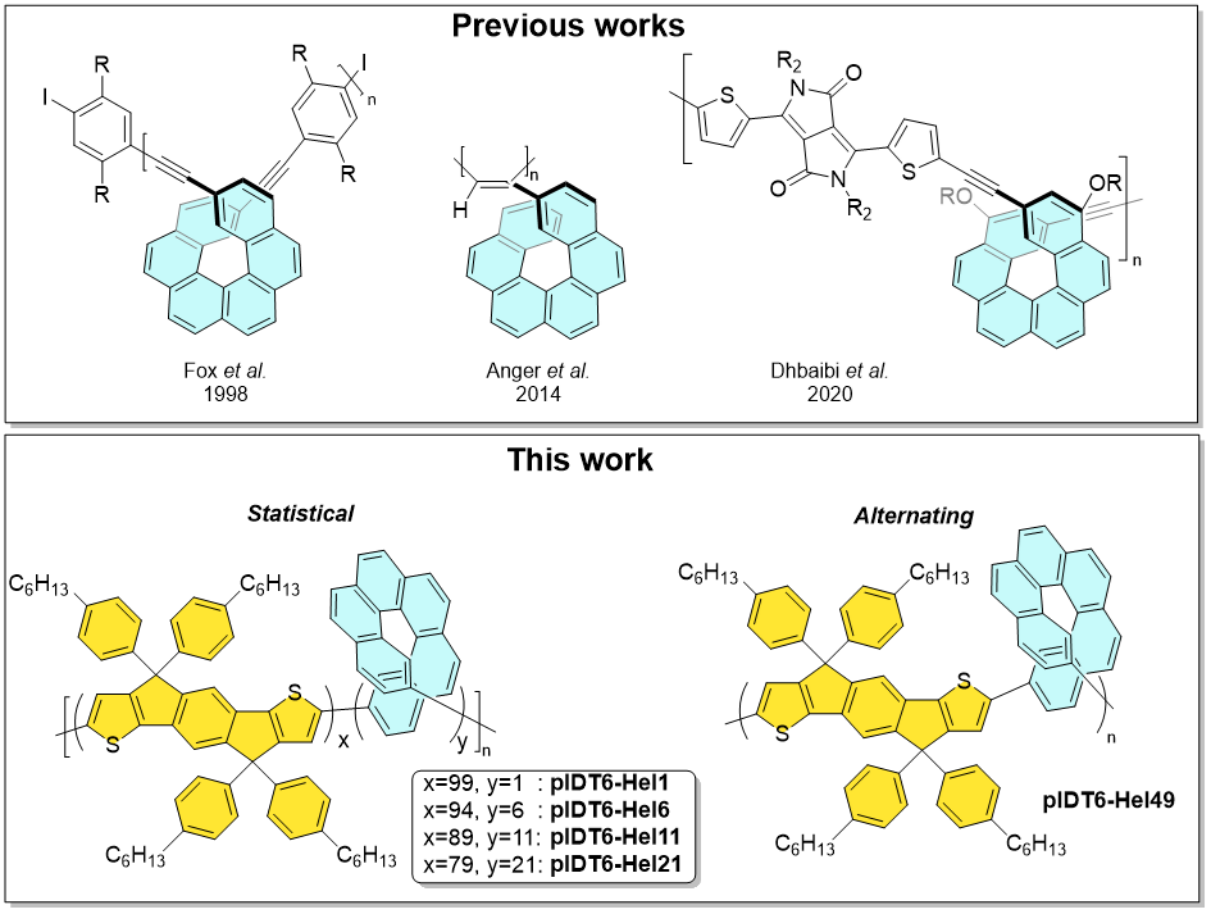

Figure 1. Chemical structures of chiral conjugated covalent polymers based on the carbo[6]helicene moiety described in the literature[12b,d,e] and general structure of the polymers developed in the present work.

Given this, it remains synthetically challenging to develop helicene-based chiral CPs possessing high molecular weight, good solubility and processability in the appropriate quantity

to accomplish a complete structure/optoelectronic properties/device performances relationships study; this aspect is still missing from the scientific community.

In this work, we present the efficient synthesis of a series of solution processable high molecular weight CPs containing either racemic or enantiopure helicenes in the polymer backbone, which allowed us to perform a detailed microscopic-macroscopic study. More specifically, we firstly evidenced how the addition of a low proportion of racemic helicene into the polymer backbone can fine tune the optical properties, energy levels and charge transporting properties of the pristine CPs, as well as impact their performances when implemented in organic photovoltaic (OPV) devices as electron donors. We then performed similar studies on the enantiopure CPs and compared the enantiopure to the racemic materials with respect to their optical properties, energy levels and charge transporting properties. We also compared enantiopure *vs*. racemic materials in OPV devices, highlighting the role of self-assembly on the macroscopic properties. To the best of our knowledge, this work represents the first reported use of chiral CPs based on main-chain chirality in a solar cell device.

2. Results and discussion

2.1. Synthesis and properties characterization of the racemic polymers

A series of polymers containing statistical amounts of 4,4,9,9-tetrakis(4-hexylphenyl)-4,9-dihydro-s-indaceno[1,2-b:5,6-b']dithiophene **IDT6** and **Hel** were synthesized from 2,15-dibromo-[6]helicene (**Hel-Br**) and the corresponding dibrominated and distannylated derivatives of **IDT6** using Stille aromatic cross-coupling polymerization conditions (see Synthesis section of the SI). Derivatives of **IDT** are known to provide wide bandgap polymers with excellent performance in devices such as OPVs[14] and OFETs.[15] They can be synthesized in a straightforward manner including a wide range of functionalities. Typical hexyl side chains were chosen on **IDT** to balance good solubility and packing, and to compensate for the low solubility of the helicene moiety.

The **Hel-Br** molar loading fraction (x) was selected to range from 10 to 50 %, with 10 % increments, through control of **IDT6-Br** stoichiometry in the reaction mixture. The homopolymer **pIDT6** was prepared as a reference polymer. The racemic and enantiopure (*P)*- and (*M*)-2,15-dibromo-carbo[6]helicene (**P/M)Hel-Br** monomers were prepared through a classical oxidative photocyclization reaction, following previously reported procedures, followed by chiral HPLC resolution (see SI part).[16] As shown in Table 1, the increase of the helicene loading in the reaction mixture (from 10 to 50 %) had a direct impact on the reaction time required to generate a polymer molecular weight that would allow for sufficient

processabilty. While the reaction was stopped after 8 minutes in the case of the homopolymer, it required one day (24 h) for the **pIDT6-Hel49** polymer.

After purification, the resulting polymers were collected from the chloroform fraction using a Soxhlet extraction. The average molecular weight per number ($\overline{M_n}$), the average molecular weight per weight ($\overline{M_w}$) and the polydispersity ($D = \overline{M_w}/\overline{M_n}$) of these polymers were estimated by Gel Permeation Chromatography (GPC, see Figure S2). Increasing the helicene loading in the reaction mixture led to polymers with lower molecular weight, despite the longer reaction times used (see Table 1). This indicates the lower reactivity of the helicene monomer in comparison to the **IDT6** moiety. We mainly attribute this to the steric hindrance of 2,15-dibromo-carbo[6]helicene, which negatively impacts the kinetics of the cross-coupling reaction and slows down the overall polymerization. For instance, racemic polymers **IDT6-Hel1** and **IDT6-Hel11** displayed a $\overline{M_w}$ of 83.5 and 13.4 kDa, respectively (which corresponds to 92 and 16 repeating units). Nevertheless, the increased reaction times enabled us to obtain high molecular weight **IDT6**-based CPs containing helicenes. It is especially noticeable that the molecular weight obtained for polymers **pIDT6-Hel1** and **pIDT6-Hel6** and their processability (all the newly prepared polymers were found readily soluble in common chlorinated solvents) are comparable to state-of-the-art (non-chiral) polymers in the literature.

The polymers were analyzed by ^{1}H-NMR spectroscopy to assess the exact proportion of helicene unit incorporated into the polymeric backbone. From Figure S1, it is clear that by increasing the 2,15-dibromo-carbo[6]helicene **HelBr** reaction loading from 10 to 50 %, the intensity of the multiplet at 7.90-8.35 ppm, typical of the helicene core, gradually increases. Interestingly, the thiophene proton peak at 6.28 ppm is influenced by the neighboring effect of the helicene. Furthermore, the signal at 2.55 ppm (corresponding to the methylene of the **IDT6** alkyl chains, see Part 3 - NMR in the SI for the full spectra) starts to split, which indicates a dissymmetric environment for these protons due to the presence of the helicene moiety. The helicene and methylene signals were used to evaluate the actual **IDT6**:**Hel** ratio in each polymer, which was found to be different from the monomer ratio in the reaction (see Table 1). Note that this NMR methodology gives approximate values since the slow relaxation times observed in NMR measurements for polymers may affect the peak intensities. As an illustrative example, the loading of 10% helicene gives access to a polymer incorporating around 1% helicene and displaying a $\overline{M_w}$ of 83.5 kDa. It was observed that only **pIDT6-Hel49** has a feed ratio equal to the observed one in the backbone, though it is also the lowest molecular weight polymer of this study. Overall, the sterically hindered **Hel-Br** unit shows low reactivity and tends to slow down

the polymer growth following its incorporation into the polymer chain, while the presence of the **IDT6-Br** co-monomer is key to achieve high molecular polymers.

Table 1. Critical parameters obtained for the **pIDT6-Hel(x)** polymers.

Polymer	Hel loading	Reaction time [min]	Hel ratio[a]	$\overline{M_w}$ [kDa]	*D*	Repeat Units	λ_{max}^{abs} [nm]^{sol}	λ_{max}^{abs} [nm]^{film}	E_g^{opt} [eV]	λ_{max}^{PL} [nm]^{sol}	PLQY [%]^{Sol}	E_{HOMO} [eV]	E_{LUMO} [eV][b]	μ_h^{SCLC} [$cm^2.V^{-1}s^{-1}$]
pIDT6	-	8	-	130.6	2.5	144	522, 558	555	2.10	568, 614	-	-5.08±0.02	-2.98	9.04 x10^{-5}
pIDT6-Hel1	10%	45	1%	83.5	4.8	92	519, 554	554	2.08	571, 614, 680	30	-5.17±0.01	-3.09	8.32 x10^{-5}
pIDT6-Hel6	20%	75	6%	27.8	3.0	32	517, 548	516	2.10	570, 613	35	-5.16±0.01	-3.06	2.10 x10^{-5}
pIDT6-Hel11	30%	165	11%	13.4	1.6	16	477, 516, 541	510	2.10	567, 607	45	-5.32±0.01	-3.22	4.30 x10^{-5}
pIDT6-Hel21	40%	360	21%	9.0	1.7	12	439, 471, 500	471	2.10	491, 559, 598	33	-5.36±0.03	-3.26	4.80 x10^{-7}
pIDT6-Hel49	50%	1440	49%	5.5	1.6	9	432, 464	437	2.41	491, 522	16	-5.57±0.02	-3.16	9.30 x10^{-9}

a) Determined by ^{1}H NMR (see spectra in Part 3 – NMR of the SI).
b) Calculated by E_{HOMO} - E_g^{opt}

The UV-Vis absorption spectra of the synthesized polymers (Figure 2a) were recorded in chloroform solution at room temperature ($c \approx 10^{-5}$ M); note that all ε and $\Delta\varepsilon$ values in this work are given in units of M^{-1} cm^{-1}. The **pIDT6**, as well as the polymers containing low helicene ratios (**pIDT6-Hel1** and **pIDT6-Hel6**), exhibit a structured band with a maximum around 558 nm and a well-resolved vibronic side band at 522 nm, characteristic of the rigid planar structure of the **IDT6** unit.[17] Interestingly, when the helicene percentage increases, a blue-shift, and a broadening of the absorption bands with lower intensity are observed (ε = 39950 for **pIDT6-Hel1** *vs.* 13100 for **pIDT6-Hel49**). This confirms that the incorporation of the helicene into the polymer chain has a strong impact on the overall polymeric structure. Concomitantly, new bands between 400-500 nm appear, originating from the helicene monomer, with increased loading of the helicene units. Overall, the polymers **pIDT6-Hel11** and **pIDT6-Hel21** containing 11% and 21 % of helicene, respectively, are the most balanced in terms of optical response, with observable absorption contributions from both **Hel** and **IDT6**.

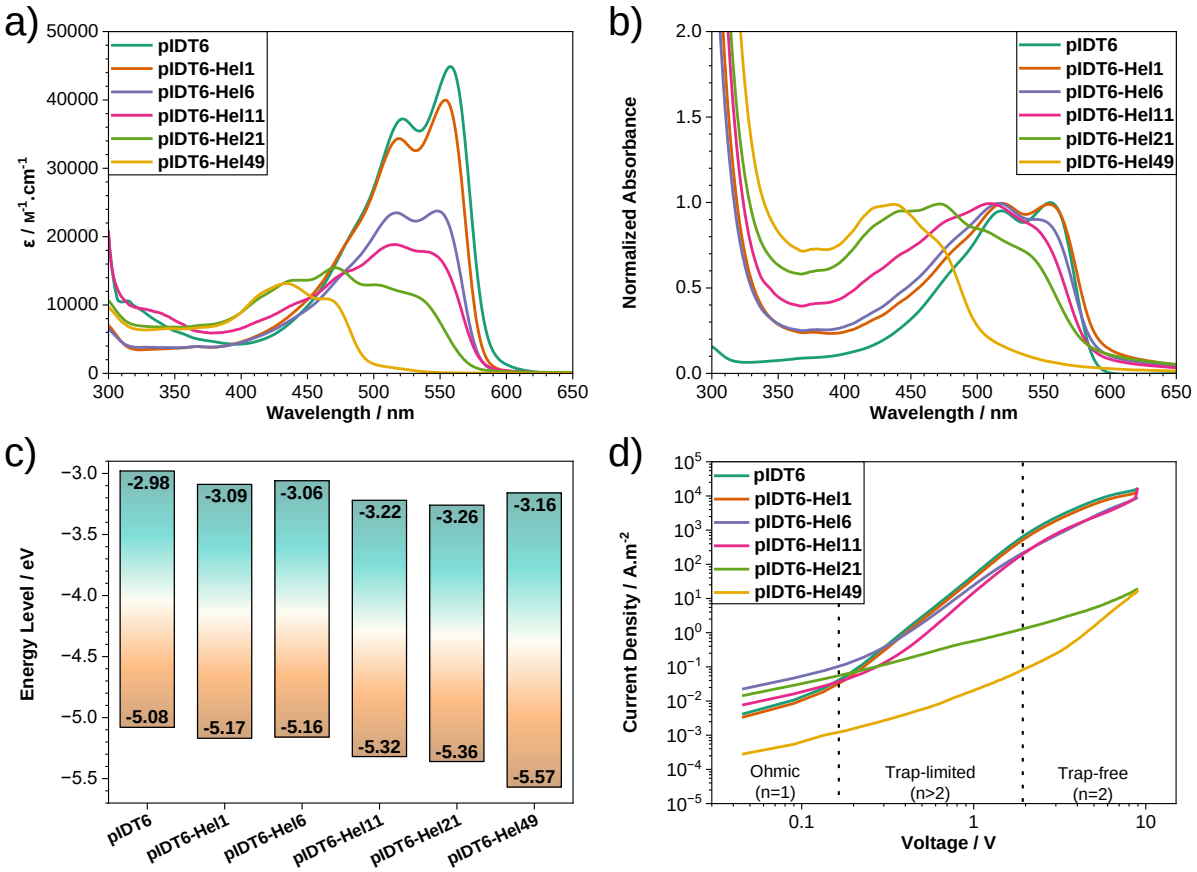

Figure 2. a) Experimental absorption spectra of **pIDT6-Hel(x)** polymers in $CHCl_3$ solutions (c = 10^{-5} M) at room temperature; b) Experimental normalized absorption spectra in solid-state spin-coated films of **pIDT6-Hel(x)** polymers at r.t.; c) Energy levels of the racemic **pIDT6-Hel(x)** polymers stemming from APS and ss-UV-Vis; d) Hole mobilities of the racemic **pIDT6-Hel(x)** polymers from SCLC measurements.

No significant differences were observed for polymer absorption between the solution (Figure 2a) and the solid-state (Figure 2b). This indicates a lack of any significant supramolecular arrangement or aggregation-induced effect, which was further supported by thermally induced absorption spectra (Figure S3). Indeed, the thermally induced absorption spectra do not show any differentiation in the absorption profiles, even at 105 °C in oDCB. The polymer bandgap was estimated based on the solid-state absorption data (Table 1).[18] It is interesting to note that the absorption offset, and thus the bandgap, remains the same throughout the whole series, *i.e.* around 2.1 eV (except the **pIDT6-Hel49** for which a 0.3 eV difference is observed). It is therefore the following trends are evident: statistical insertion of the helicene monomer results in the same absorption maxima and bandgap as pure **pIDT6** up to 11% loading. Broadening of the absorption spectra with a blue shift of the absorption maxima is observed up to 21% loading, but without a change in bandgap. A significant blue shift and simultaneous widening of the bandgap is observed at 49% loading. These results can be explained by

considering how the different compositions and main chain positioning of the helicene in the polymer backbone affects intramolecular charge transfer (ICT).

The emission properties of the polymers were also studied both in solution and as thin films (Table 1 and Figures S4 and S5). In solution, upon excitation at 365 nm, an efficient energy transfer from helicene to the IDT occurs. The characteristic vibronic feature of the **pIDT6** is shown in the helicene-based IDT CPs up to 11% helicene content (**pIDT6-Hel1** and **pIDT6-Hel11**, with the emission wavelength λ_{max}^{PL} within the range of 567-571 nm. The same vibronic feature is also present in the **pIDT6-Hel49** but blue shifted, with λ_{max}^{PL} at 491 nm (Figure S4). Interestingly, the **pIDT6-Hel21** exhibits slightly blue shifted λ_{max}^{PL} (559 nm) with an additional small peak at 491 nm, as observed for **pIDT6-Hel49**. The photoluminescence quantum yields (PLQY) also present an interesting trend. Upon increasing the helicene content up to 11%, the PLQY gradually increases from 30% to 45% and then gradually decreases to 33% and 16% for the **pIDT6-Hel21** and **pIDT6-Hel49**, respectively. Passing from solution to the solid state, polymer emission is much less intense, where only the **pIDT6-Hel21** and **pIDT6-Hel49** exhibit a photoluminescence signal (see Figure S5), with λ_{max}^{PL} of 660 nm and 605 nm for the **pIDT6-Hel21** and **pIDT6-Hel49**, respectively. As in solution, efficient energy transfer from helicene to the IDT occurs for **pIDT6-Hel21** and **pIDT6-Hel49**, whereas the aggregation of the IDT seems to be much stronger with lower helicene loadings resulting in significant photoluminescence quenching.

The E_{HOMO} of the CPs levels were determined by Ambient pressure Photoemission Spectroscopy (APS) using a Kelvin probe (see APS part in the SI)[19] whereas the E_{LUMO} levels were estimated by deducing the bandgap obtained from solid-state absorption spectra on the E_{HOMO} levels. To our surprise, the introduction of even 1 % of **Hel** has a strong impact on the E_{HOMO} values (-5.08 eV for **pIDT6** *vs.* -5.17 eV for **pIDT6-Hel1**) which can be attributed to the deeper E_{HOMO} level and the weaker electron donating nature of **Hel** as compared to **IDT** (Figure S7). As shown in Table 2 and in Figure 2c, the energy levels and bandgaps do not change significantly for **pIDT6-Hel1/pIDT6-Hel6** which contain below 10% loading of the helicene. As the content of the helicene increases to 11% and 21% for **pIDT6-Hel11** and **pIDT6-Hel21**, respectively, the E_{HOMO} level further decreases by ~0.2 eV (-5.32 and -5.36 eV, respectively), without altering the optical bandgap. Finally, for the **pIDT6-Hel49** the E_{HOMO} strongly decreases to nearly -5.6 eV with an increase in bandgap. Thus, for this specific series of polymers a small amount of helicene up to 21% can decrease the E_{HOMO} which can be beneficial on the open circuit voltages (V_{oc} values) in OPVs, without negatively impacting the optical bandgap (only a small blue shift on the absorption maxima).

To correlate the increased composition of the helicene in the backbone of the pristine CPs with a macroscopic property, we performed a detailed study on their charge transporting properties by space charge limited current (SCLC) and the results are shown in Table 1 and in Figure 2d. Since these polymers will be employed as electron donor polymers in OPVs we focused our attention on hole mobility (μ_h). Polymers **pIDT6** and **pIDT6-Hel1** exhibit a higher μ_h which approaches 10^{-4} $cm^2.V^{-1}s^{-1}$ ($9.04x10^{-5}$ $cm^2.V^{-1}s^{-1}$ for **pIDT6** and $8.32x10^{-5}$ $cm^2.V^{-1}s^{-1}$ for **pIDT6-Hel1**), which is similar to the high-performance CPs reported in the literature.[20] The fact that the **pIDT6-Hel1** presents similar μ_h to **pIDT6** demonstrates that 1% of **Hel** does not prevent the **pIDT6-Hel1** from adopting a similar self-assembly process as **pIDT6**. As the presence of helicene increases (6% and 11%) in the polymer backbone, **pIDT6-Hel6** and **pIDT-Hel11** maintain μ_h in the order of 10^{-5} $cm^2.V^{-1}s^{-1}$, whereas further increase of the helicene content to 21% reveals a significant decrease of the μ_h by two orders of magnitude ($4.8x10^{-7}$ $cm^2.V^{-1}s^{-1}$ for **pIDT6-Hel21**). Since there is not a large difference between the $\overline{M_w}$ of the **pIDT-Hel11** and **pIDT-Hel21** this significant decrease in μ_h can be attributed to the increased content of the helicene. Finally, **pIDT-Hel49** presents the lowest μ_h which is in the order of 10^{-9} $cm^2.V^{-1}s^{-1}$. This likely arises from the very low $\overline{M_w}$, resulting in poor thin film quality, as well as the additional helicene content.

2.2. Synthesis and properties characterization of the enantiopure polymers

Having analyzed in detail the whole series of racemic helicene IDT CPs with the purpose of studying the effect of main chain helicene loading on CP microscopic and macroscopic properties (μ_h and OPV performances), we decided to generate enantiopure analogues of **pIDT6-Hel1** and **pIDT6-Hel11**. The (*P*) and (*M*) enantiomers of 2,15-dibromo-carbo[6]helicene, namely **PHel** and **MHel**, were readily obtained using HPLC over a chiral stationary phase. The same procedures as for the racemic polymers were used to synthesize and characterize the corresponding enantiopure **pIDT6-Hel1** and **pIDT6-Hel11** (see Part 2 - Synthesis in the SI). The obtained enantiopure polymers share most of the features of their racemic comparators, such as the same helicene loading in the backbone (1 % and 11 % respectively, as checked by ^{1}H NMR) and similar molecular weights (Table 2).

Table 2. Critical parameters obtained for the enantiopure **pIDT6-(P/M)Hel(x)** polymers.

Polymer	$\overline{M_w}$ [kDa]	*D*	λ_{max}^{sol} [nm]	λ_{max}^{film} [nm]	E_g^{opt} [eV]	E_{HOMO} [eV]	E_{LUMO} [eV]	μ_h^{SCLC} [$cm^2.V^{-1}s^{-1}$]
pIDT6-PHel1	89.4	5.7	553	558	2.09	-5.19±0.03	-3.10	3.28×10^{-5}
pIDT6-MHel1	91.2	5.8	553	559	2.08	-5.12±0.02	-3.04	4.01×10^{-5}
pIDT6-PHel11	10.1	1.5	511	516	2.09	-5.29±0.02	-3.20	5.62×10^{-5}
pIDT6-MHel11	11.2	1.4	511	515	2.10	-5.27±0.02	-3.17	7.59×10^{-6}

Interestingly, the GPC chromatograms of the enantiopure *vs.* the racemic polymers (Figure S8) present slight differences as the content of the enantiopure helicene increases (from 1% to 11%). While for 1% helicene loading the GPC chromatograms of racemic *vs*. enantiopure polymers are almost identical (Figure S8a), for 11% helicene loading there are slight differences (Figure S8b). This provides evidence that polymers with 1% helicene exhibit similar self-assembly between the enantiopure and racemic analogues whereas different self-assembly process (enantiopure *vs*. racemic) are present at 11% loading. However, both the enantiopure (**pIDT6-(P/M)Hel1**, **pIDT6-(P/M)Hel11)** and the racemic (**pIDT6-Hel1** and **pIDT6-Hel11**) polymers present similar microscopic properties (absorption spectra, bandgap, energy levels) for analogous helicene content (Tables 1 and 2).

To verify that the obtained polymers did not undergo a loss in enantiopurity through the cross-coupling reaction, ECD spectroscopic analyses were carried out (see Figures 3a-d). The racemic helicene CPs are, unsurprisingly, ECD-silent, whereas the enantiopure samples have almost mirror-image responses. The signals of **pIDT6-(*P*/*M*)Hel1** in solution (Figure 3a) and solid state (Figure 3c) were found noisy and of low intensity ($\Delta\varepsilon$ values below 100 $M^{-1}.cm^{-1}$ in the helicene absorption region in solution) and the helicene loading was found not sufficient to induce chirality to the IDT chromophore (no ECD-active band in the IDT absorption region).

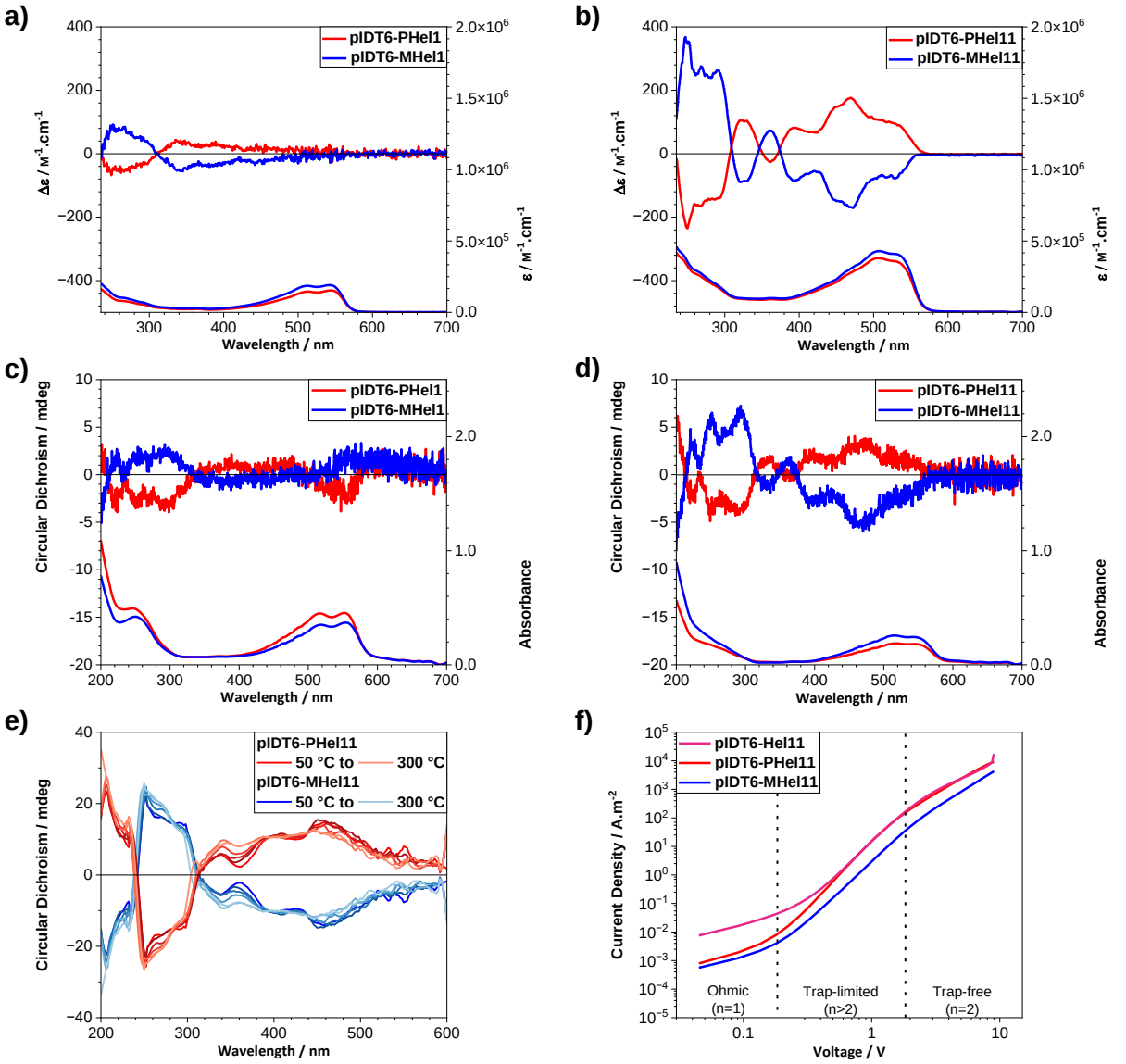

Figure 3. a) ECD (top) and UV-Vis absorption spectra (bottom) of the chiral **pIDT6-(P/M)Hel1** and b) **pIDT6-(P/M)Hel11** polymers in dichloromethane solution at room temperature (c 6 x 10^{-6} and 1 x 10^{-5} M, respectively taking into account $\overline{M_n}$ average molecular weight); c) ECD (top) and UV-Vis absorption spectra (bottom) of the thin-films of **pIDT6-(P/M)Hel1** and d) **pIDT6-(P/M)Hel11**; e) Circular dichroism in thin films of **pIDT6-(P/M)Hel11** after a temperature ramp from 50 °C to 300 °C (10 °C/min, 3 min incubation, intermediate curves are omitted for clarity); f) hole mobilities of the **pIDT6-Hel11** based polymers.

The situation is totally different for **pIDT6-(P/M)Hel11** both in solution (Figure 3b) and in solid state (Figure 3d) where the ECD response is not solely from the helicene unit.[21] Indeed, **pIDT6-PHel11** in Figure 3b shows two strong negative bands between 250-300 nm ($|\Delta\varepsilon|$ up to 200-300 $M^{-1}.cm^{-1}$) attributable to the π-π* transitions within the helicene. Two additional bands of lower intensity appear at longer wavelengths, a positive one at 330 nm ($\Delta\varepsilon$ ~ +105 $M^{-1}.cm^{-1}$) and a negative one at 360 nm ($\Delta\varepsilon$ ~-27 $M^{-1}.cm^{-1}$). A set of three intense positive

bands, from 390 to 570 nm, are also observed ($\Delta\varepsilon$ up to 180 M $^{-1}$.cm^{-1}). Interestingly, this ECD signature, which increases with the **Hel** content, corresponds to the absorption region of the **IDT6** unit, thus indicating transfer of the chiroptical response from the chiral helicene to the achiral **IDT6** unit. For the (*M*)-enantiomer, higher $\Delta\varepsilon$ values were observed. Note that dissymmetry factors in absorption and emission are in the typical range of chiral organic materials (g_{abs} up to 1.4×10^{-3} in the helicene part and 1.0×10^{-3} for the **IDT6** region, see Figure S9). The same profile is also present in the solid state with lower intensity and slightly increased noise.

Samples of **pIDT6-(P/M)Hel11** were further examined at the Diamond synchrotron beamline number 23 for advanced chiroptical analyses (Figure 3e).[22] The two enantiopure polymers as thin films were found to have an ECD profile very similar to the solution and solid state (Figures 3b, 3d), suggesting intrachain chirality as the source of chiroptical activity. It is interesting to note that some increase in the ECD signal was observed upon heating, especially in the 260 and the 360 nm region of the spectra. This may possibly originate from the presence of the helicene in the backbone that constrains the polymeric chain movements.

To correlate the different structure of the enantiopure **pIDT6-(P/M)Hel1** and **pIDT6-(P/M)Hel11** samples in the solid state with a macroscopic property, we measured their hole mobilities (μ_h) by SCLC (Table 2 and Figure 3f). The (*P*) and (*M*) enantiomers of **pIDT6-Hel1** exhibit very similar μ_h of 3.28×10^{-5} cm^2.V^{-1}s^{-1} and 4.01×10^{-5} cm^2.V^{-1}s^{-1}, respectively (Figure S10), which is also very similar to the racemic comparator. On the contrary, the (*P*) and (*M*) enantiomers of **pIDT6-Hel11** exhibit distinct μ_h (Figure 3f). The **pIDT6-PHel11** exhibits μ_h of 5.62×10^{-5} cm^2.V^{-1}s^{-1} that is slightly higher than the racemic analogue (4.30×10^{-5} cm^2.V^{-1}s^{-1}), whereas the **pIDT6-MHel11** exhibits μ_h of 7.59×10^{-6} cm^2.V^{-1}s^{-1}, which is one order of magnitude lower. Therefore, it is evident that upon insertion of 1% **Hel** (either in racemic or enantiopure forms) the obtained μ_h are similar and close to the homopolymer. This indicates that addition of 1 **Hel** moiety over 100 indacenodithiophene units does not significantly affect the self-assembly process of the polymers and all the 1% polymers as thin films will result to similar μ_h (in agreement to the GPC findings of Figure S8a). Then increasing the insertion of **Hel** to 11% in the polymer backbone, the obtained μ_h are not similar even for the enantiopure derivatives. This shows now that the addition of 1 **Hel** moiety every 10 indacenodithiophene units (and especially the positioning/sequence within the repeat unit as they are statistical polymers) plays a more important role on the self-assembly process of the polymers (again in agreement with the GPC findings in Figure S8b).

2.3. Organic Photovoltaic (OPV) characterization of the racemic and enantiopure polymers

To continue further the detailed microscopic to macroscopic relationship study on both the racemic and chiral CPs, we examined their performance in heterojunction OPVs (Figures 4a-b). As a non-fullerene acceptor, the well-studied **IO4Cl** was utilized given its wide bandgap and favorable E_{HOMO} level, which provides the required offset of ~0.5 eV[23] for exciton dissociation (Figure S11) for most of the synthesized racemic (**pIDT6-Hel1, pIDT6-Hel6, pIDT6-Hel11)** and enantiopure polymers (**pIDT6-(P/M)Hel1, pIDT6-(P/M)Hel11)**.

We fabricated OPVs in a conventional architecture (Figure S11) based on ITO/PEDOT/active layer/Na-DPO/Ag. We first measured the current density-voltage (*J*-*V*) characteristics of blends comprising of the reference polymer **IDT6** and the racemic polymers **pIDT6-Hel1 – pIDT6-Hel6 - pIDT6-Hel11** under AM1.5G illumination (Figure 4a). As summarized in Table 3, **pIDT6**:**IO4Cl**-based solar cells delivered a power conversion efficiency (PCE) up to 4.1 %, together with an open-circuitt voltage (V_{oc}) of 1.02 V, a short-circuit current density (J_{sc}) of 7.92 mA.cm^{-2} and a fill factor (FF) of 51.7 %. Interestingly, **pIDT-Hel1-**based devices showed similar performance (PCE of 4 %), whereas higher loading of helicene leads to reduced efficiency, mainly attributed to lower FF values (Figure 4b and Figure S12).

We then turned our attention to the different performances of racemic and enantiopure **pIDT6-Hel1**-based devices. We first verified the ECD response of the enantiopure blends and found no ECD response in the absorption region of the IO4Cl unit, i.e. around 600-700 nm (see Figures 4c,4d). Figure 4e shows the *J*-*V*s under one sun illumination of **pIDT6-Hel1**:**IO4Cl**, **pIDT6-PHel1**:**IO4Cl** and **pIDT6-MHel1**:**IO4Cl**-based OPVs. The PCE increased to 4.5 % and 4.8 % for **pIDT6-PHel1**:**IO4Cl** and **pIDT6-MHel1**:**IO4Cl**, respectively (Figures 4b,e and Figure S13). These improved performances are mainly attributed to higher J_{sc} values of 8.55 mA.cm^{-2} and 8.70 mA.cm^{-2} for **pIDT6-PHel1**:**IO4Cl** and **pIDT6-MHel1**:**IO4Cl**, respectively, compared to the racemic blend (Figure S13c).

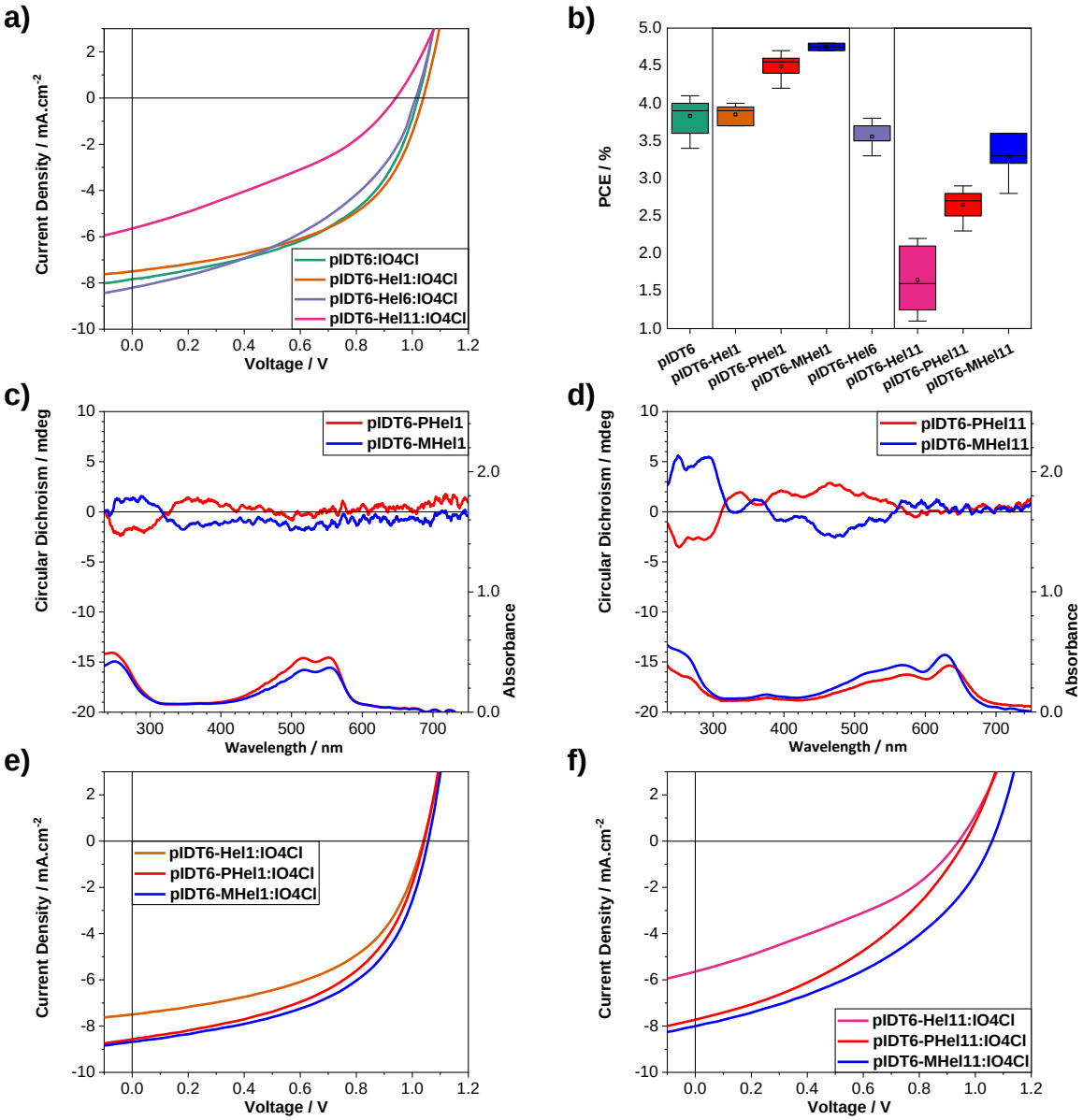

Figure 4. (a) *J-V* curves of the cells based on racemic polymers, (b) box plot of the PCE of all the solar cells studied. (c, d) ECD (top) and UV-Vis absorption spectra (bottom) of the thin-films blends of **pIDT6-(P/M)Hel1:IO4Cl** (c) and **pIDT6-(P/M)Hel11:IO4Cl** (d). (e, f) *J-V* curves of the cells based on racemic and enantiopure polymers on 1% helicene loading (e) and on 11% helicene loading (f).

Table 3. Average and best performances of **pIDT6-Hel(x)** cells.

Active layer	PCE [%]	PCE (ave.) [a]	V_{oc} [V]	V_{oc} (ave.) [a]	J_{sc} [mA.cm^{-2}]	J_{sc} (ave.) [a]	Fill Factor (FF)	Fill Factor (ave.) [a]
pIDT6:IO4Cl	4.1	3.8	1.02	1.00	7.92	7.64	51.7	49.3
pIDT6-Hel1:IO4Cl	4.0	3.9	1.04	1.04	7.56	7.29	52.2	50.5
pIDT6-Hel6:IO4Cl	3.8	3.6	1.03	1.03	8.21	7.91	46.7	43.6
pIDT6-Hel11:IO4Cl	2.2	1.7	0.95	0.78	6.33	5.63	38.4	34.8

To gain information on the charge transport properties of the racemic and enantiopure **pIDT6-Hel1**-based blends, we calculated the charge carrier mobility with the SCLC method (Figure S14).[24] The *J*-*V* characteristics of hole and electron-only devices are depicted in Figures S15a and S15b, and the calculated mobility values are collected in Table S6. Racemic and enantiopure polymer blends clearly delivered similar hole mobility values of 3.4×10^{-4} cm^2.V^{-1}s^{-1} and 2.5×10^{-4} cm^2.V^{-1}s^{-1} respectively, in line with the similar FF values obtained. Therefore, the improved performance observed for enantiopure devices should reflect a better light-to-current conversion. For this reason, we measured the external quantum efficiency (EQE). Figure S16 shows the EQE of **pIDT6-Hel1**:**IO4Cl**, **pIDT6-PHel1**:**IO4Cl** and **pIDT6-MHel1**:**IO4Cl**. It is evident that **pIDT6-PHel1**:**IO4Cl** and **pIDT6-MHel1**:**IO4Cl** showed higher EQE in the entire spectrum range. The reasoning behind this result is beyond the scope of this work, however we speculate that the improved J_{sc} in the enantiopure devices should be related to purer donor:acceptor domains or reduced domain sizes rather than changes in microstructure.[25,26] Preliminary atomic force microscopy (AFM) results (Figure S17) support this argument because there are no significant morphological changes between the studied blends, only variation on the surface roughness.

Similar trends in the PCE increase as in the case of the racemic and enantiopure **pIDT6-Hel1**-based devices is also observed in the case of the racemic and enantiopure **pIDT6-Hel11**-based OPV devices. Figure 4f shows the *J*-*V*s under one sun illumination of **pIDT6-Hel11**:**IO4Cl**, **pIDT6-PHel11**:**IO4Cl** and **pIDT6-MHel11**:**IO4Cl**-based OPVs. The PCE from 1.7 % for the racemic **pIDT6-Hel11**:**IO4Cl** increased to 2.7 % and 3.3 % for **pIDT6-PHel11**:**IO4Cl** and **pIDT6-MHel11**:**IO4Cl**, respectively. Herein, the improved performances are mainly attributed to both the higher J_{sc} values of 7.01 mA.cm^{-2} and 7.64 mA.cm^{-2} for **pIDT6-PHel1**:**IO4Cl** and **pIDT6-MHel1**:**IO4Cl**, respectively, compared to the racemic blend

and the increased V_{oc} of the **pIDT6-MHel11**:**IO4Cl** based devices versus the other enantiomeric form (**pIDT6-PHel11**:**IO4Cl**) and the racemic (**pIDT6-Hel11**:**IO4Cl**).

Intriguingly, in all the studied chiral polymer:**IO4Cl** blends within this work all the experimental findings show that the (*M*)-enantiomer CP presents increased photovoltaic performance in the two loadings (1% and 11%) than the (*P*)-enantiomer CP. This indicates a much-improved compatibility of the polymers containing the (*M*)-enantiomer with the **IO4Cl**, mainly again as a result of different statistical contents or helicene sequence/positioning. The exact origin of such differences will thus be very interesting to analyze in the future, however not within the scope of this work.

3. Conclusions

A new methodology for the development of CPs with main chain chirality and high average molecular weight is demonstrated by synthesizing statistical or alternating CPs containing helicene **Hel** and indacenodithiophene **IDT** building blocks. This method can pave the way for the implementation of chiral helicenes or other chiral conjugated building blocks in the field of CPs. A detailed correlation between their microscopic - macroscopic properties has been achieved. Several trends linked to the loading of helicene are evident, such as polymer molecular weight dependence, absorption and emission properties, energy level deepening, ECD responses, charge-carrier mobilities and OPV performance. The most important outcome is that the macroscopic properties of the chiral CPs are affected by both the content and the enantiomeric form of the **Hel** in the polymer backbone. In particular, it is demonstrated that the enantiopure derivatives of the 11% statistical chiral **pIDT6-Hel11** exhibit different μ_h *vs* the racemic samples, whereas such a trend is not apparent for the corresponding 1% helicene loading and between the two enantiomeric forms as well. In addition, it is demonstrated that enantiopure CPs show superior photovoltaic performance over their racemic counterparts. For example, a 20 % increase in the PCE is observed for enantiopure polymers incorporating only 1 % of chiral helicene loading in comparison to **IDT6** homopolymers and racemic systems. Interestingly, in our studied systems the polymers with the (*M*)-enantiomer (**pIDT6-MHel1, pIDT6-MHel11)** exhibit higher photovoltaic performances *vs* their (*P*)-enantiomer analogues (**pIDT6-PHel1, pIDT6-PHel11)**.

We anticipate that this methodology will be a source of new inspiration for synthetic chemists to design and synthesize new solution processable high molecular weight CPs with main chain chirality especially in the field of OPVs as new electron donor polymers, but also in the domain of photodetectors. In addition, we believe that the obtained results will inspire

physical chemists/material scientists to study in detail the origins of differing self-assembly processes in the solid state for this new family of materials (CPs with main chain chirality) and how this relates to the resulting microstructures. Such insight would provide new guidelines for obtaining novel CPs with controlled or pre-determined microstructures that will boost performance in various optoelectronic applications.

Supporting Information

Supporting Information is available from the Wiley Online Library or from the author.

Acknowledgements

The European Commission Research Executive Agency (Grant Agreement Number 859752 – HEL4CHIROLED – H2020-MSCA-ITN-2019) is thanked for financial support. M.J.F. would like to thank the Engineering and Physical Sciences Research Council for funding (EP/R00188X/1). J.C. acknowledges the Centre National de la Recherche Scientifique (CNRS), and the University of Rennes. C.L.C acknowledges the Hellenic Foundation for Research and Innovation (H.F.R.I.) under the "2nd Call for H.F.R.I. Research Projects to support Faculty Members & Researchers" (Project Number: 4694). The authors would also like to thank Diamond Light Source for beamtime, and the staff of beamline B23 for assistance and data collection. Dr. Monika Srebro-Hooper is warmly thanked for providing calculated HOMO-LUMO levels.

Received: ((will be filled in by the editorial staff))
Revised: ((will be filled in by the editorial staff))
Published online: ((will be filled in by the editorial staff))

References

[1] a) A. Facchetti, *Chem. Mater.* **2011**, *23* (3), 733–758; b) M. Leclerc, J.-F. Morin, Eds.; *Synthetic Methods for Conjugated Polymers and Carbon Materials*; Wiley-VCH Verlag GmbH & Co. KGaA: Weinheim, Germany, **2017**; c) K. Gu, Y. Loo, *J. Polym. Sci. Part B: Polym. Phys.* **2019**, *57*, 1559–1571; d) R. M. Pankow, B. C. Thompson, *Polymer* **2020**, *207*, 122874; e) H. Lu, X. Li, Q. Lei, *Front. Chem.* **2021**, *9*, 732132.

[2] a) T. Nakano, Y. Okamoto, *Chem. Rev.* **2001**, *101*, 4013–4038; b) E. Yashima, N. Ousaka, D. Taura, K. Shimomura, T. Ikai, K. Maeda, *Chem. Rev.* **2016**, *116*, 13752–13990; c) F. Freire, E. Quiñoá, R. Riguera, *Chem. Rev.* **2016**, *116*, 1242–1271; d) M. Verswyvel, G. Koeckelberghs,

Polym. Chem. **2012**, *3*, 3203–3216; e) R. Abbel, A. P. H. J. Schenning, E. W. Meijer, *Macromolecules* **2008**, *41*, 7497–7504; f) Y. Yang, R. Correa da Costa, D. -M. Smilgies , A. J. Campbell, M. J. Fuchter, *Adv. Mater.* **2013**, *25*, 2624–2628; g) C. Kulkarni, S. C. J. Meskers, A. R. A. Palmans, E. W. Meijer, *Macromolecules* **2018**, *51*, 5883–5890; h) L. Liu, Y. Yang**,** Y. Wang, M. A. Adil, Y. Zhao, J. Zhang, K. Chen, D. Deng, H. Zhang, K. Amin, Y. Wu, Y. Zhang**,** Z. Wei**,** *ACS Materials Lett.* **2022**, *4*, 401–409; i) L. Liu, Y. Yang, L. Zhu, J. Zhang, K. Chen, Z. Wei, *Small* **2022**, *18*, 2202941; j) L. Liu, Z. Wei, S. C. J. Meskers, *Adv. Mater.* **2023**, *35*, 2209730.

[3] T. Yamamoto, T. Yamada,Y. Nagata, M. Suginome, *J. Am. Chem. Soc*. **2010**,132, 7899–7901.

[4] J. Shen, Y. Okamoto, *Chem. Rev*. **2016**, 116, 1094–1138.

[5] E. Yashima, K. Maeda, H. Iida, Y. Furusho, K. Nagai, *Chem. Rev.* **2009,** *109*, 6102–6211.

[6] a) L. A. P. Kane-Maguire, G. G. Wallace, *Chem. Soc. Rev*. **2010**, 39, 2545–2576; b) C. Zhou, X. Sun, J. Han, *Mater. Chem. Front.* **2020**, 4, 2499–2516.

[7] a) D. Di Nuzzo, C. Kulkarni, B. Zhao, E. Smolinsky, F. Tassinari, S. C. J. Meskers, R. Naaman, E. W. Meijer, R. H. Friend, *ACS Nano* **2017**, *11*, 12713–12722; b) S. Yang, S. Zhang, F. Hu, J. Han, F. Li, *Coord. Chem. Rev.* **2023**, *485*, 215116; c) H. Zhong, B. Zhao, J. Deng, *Adv. Optical Mater.* **2023**, *11*, 2202787; d) J. R. Brandt, F. Salerno, M. J. Fuchter, *Nature Rev. Chem.* **2017**, *1*, 0045.

[8] a) R. Naaman, D. H. Waldeck, *J. Phys. Chem. Lett.* **2012**, *3*, 2178–2187; b) P. C. Mondal, N. Kantor-Uriel, S. P. Mathew, F. Tassinari, C. Fontanesi, R. Naaman, *Adv. Mater.* **2015**, *27*, 1924–1927; c) S. Mishra, A. K. Mondal, E. Z. B. Smolinsky, R. Naaman, K. Maeda, T. Nishimura, T.Taniguchi, T. Yoshida, K. Takayama, E. Yashima, *Angew. Chem. Int. Ed.* **2020**, *59*, 14671–14676.

[9] P. Wang, I. Jeon, Z. Lin, M. D. Peeks, S. Savagatrup, S. E. Kooi, T. Van Voorhis, T. M. Swager, *J. Am. Chem. Soc.* **2018**, 140, 6501–6508

[10] a) C. -F. Chen, Y. Shen, *Helicene Chemistry: From Synthesis to Applications*, 1st ed.; Springer Berlin Heidelberg: Imprint: Springer: Berlin, Heidelberg, **2017**; b) M. Gingras, *Chem. Soc. Rev.* **2013**, *42*, 968–1006; c) *Helicenes: Synthesis, Properties, and Applications*; J. Crassous, I. G., Stará, I. Starý, Eds.; Wiley-VCH: Weinheim, Germany, **2022**.

[11] K. Dhbaibi, L. Favereau, J. Crassous, *Chem. Rev.* **2019**, *119*, 8846–8953.

[12] Enantiopure fully conjugated helicene-based polymers: a) Y. Dai, T. J. Katz, *J. Org. Chem.* **1997**, *62*, 1274–1285; b) J. M. Fox, D. Lin, Y. Itagaki, T. Fujita, *J. Org. Chem.* **1998**, *63*, 2031–2038; c) H. Sugiura, Y. Nigorikawa, Y. Saiki, K. Nakamura, M. Yamaguchi, M. *J. Am. Chem. Soc*. **2004**, *126*, 14858–14864; d) E. Anger, H. Iida, T. Yamaguchi, K. Hayashi, D. Kumano, J.

Crassous, N. Vanthuyne, C. Roussel, E. Yashima, *Polymer Chemistry* **2014**, ***5***, 4909-4914; e) K. Dhbaibi, C. Shen, M. Jean, N. Vanthuyne, T. Roisnel, M. Górecki, B. Jamoussi, L. Favereau, J. Crassous, *Front. Chem.* **2020**, *8*, 237; examples of enantiopure non-fully conjugated polymers incorporating helicenes: f) A. Al Mousawi, M. Schmitt, F. Dumur, J. Ouyang, L. Favereau, V. Dorcet, N. Vanthuyne, P. Garra, J. Toufaily, T. Hamieh, B. Graff, J. -P. Fouassier, D. Gigmes, J. Crassous, J. Lalevée, *Macromolecules* **2018**, *51*, 5628–5637; g) T. Ikai, S. Anzai, K. Oki, E. Yashima, *J. Polym. Sci.* **2023**, *61*, 912–919; h) K. Fujikata, M. Gon, K. Tanaka, Y. Chujo, A. Tsurusaki, K. Kamikawa, *Macromolecules* **2023**, 56, 4550−4555; racemic π-conjugated polymers : i) F. Fenili, C. Rigamonti, A. Bossi, P. Ferruti, A. Manfredi, S. Maiorana, C. Baldoli, S. Cauteruccio, E. Licandro, E. Ranucci, *J. Polym. Sci. Part A* **2010**, *48*, 4704–4710; j) J. Hrbac, J. Storch, V. Halouzka, V. Cirkva, P. Matejkad, J. Vacek, *RSC Adv.* **2014**, *4*, 46102–46105.

[13] Helicene-based small oligomers : a) C. Schaack, E. Sidler, N. Trapp, F. Diederich, *Chem. Eur. J.* **2017**, *23*, 14153–14157 ; b) J. Vacek, J. Hrbáč, T. Strašák, V. Církva, J. Sýkora , L. Fekete, J. Pokorný, J. Bulíř, M. Hromadová, J. Crassous, J. Storch, *ChemElectroChem* **2018**, *5*, 2080–2088; c) X. Xiao, Q. Cheng, S. T. Bao, Z. Jin, S. Sun, H. Jiang, M. L. Steigerwald, C. Nuckolls, *J. Am. Chem. Soc.* **2022**, *144*, 20214−20220.

[14] a) I. McCulloch, R. S.; Ashraf, L. Biniek, H. Bronstein, C. Combe, J. E. Donaghey, D. I. James, C. B. Nielsen, B. C. Schroeder, W. Zhang, *Acc. Chem. Res.* **2012**, *45*, 714–722; b) D. Venkateshvaran, M. Nikolka, A. Sadhanala, V. Lemaur, M. Zelazny, M. Kepa, M. Hurhangee, A. J. Kronemeijer, V. Pecunia, I. Nasrallah, I. Romanov, K. Broch, I. McCulloch, D. Emin, Y. Olivier, J. Cornil, D. Beljonne, H. Sirringhaus, *Nature* **2014**, *515*, 384–388; c) Y. Li, M. Gu, Z. Pan, B. Zhang, X. Yang, J. Gu, Y. Chen, *J. Mater. Chem. A* **2017**, *5*, 10798–10814; d) Y. Li, W. K.; Tatum, J. W. Onorato, S. D. Barajas, Y. Y. Yang, C. K. Luscombe, *Polym. Chem.* **2017**, *8*, 5185–5193.

[15] X. Zhang, H. Bronstein, A. J. Kronemeijer, J. Smith, Y. Kim, R. J. Kline, L. J. Richter, T. D. Anthopoulos, H. Sirringhaus, K. Song, M. Heeney, W. Zhang, I. McCulloch, D. M. DeLongchamp, *Nat Commun* **2013**, *4*, 2238.

[16] a) M. Nakazaki, K. Yamamoto, T. Ikeda, T. Kitsuki, Y. Okamoto, *J. Chem. Soc., Chem. Commun.* **1983**, 787–788; b) T. R. Schulte, J. J. Holstein, G. H. Clever, *Angew. Chem. Int. Ed.* **2019**, *58*, 5562–5566.

[17] D. Adamczak, H. Komber, A. Illy, A. D. Scaccabarozzi, M. Caironi, M. Sommer, *Macromolecules* **2019**, *52*, 7251–7259.

[18] A. M. Wallace, C. Curiac, J. H. Delcamp, R. C. Fortenberry, *Journal of Quantitative Spectroscopy and Radiative Transfer* **2021**, *265*, 107544. 4

[19] J. R. Harwell, T. K. Baikie, I. D. Baikie, J. L. Payne, C. Ni, J. T. S. Irvine, G. A. Turnbull, I. D. W. Samuel, *Phys. Chem. Chem. Phys.* **2016**, *18*, 19738–19745.

[20] a) J. C. Aguirre, C. Arntsen, S. Hernandez, R. Huber, A. M. Nardes, M. Halim, D. Kilbride, Y. Rubin, S. H. Tolbert, N. Kopidakis, B. J. Schwartz, D. Neuhauser, *Adv. Funct. Mater.* **2014**, *24*, 784–792; b) M. Nikolka, K. Broch, J. Armitage, D. Hanifi, P. J. Nowack, D. Venkateshvaran, A. Sadhanala, J. Saska, M. Mascal, S.-H. Jung, J.-K. Lee, I. McCulloch, A. Salleo, H. Sirringhaus, *Nat. Commun.* **2019**, *10*, 2122; c) S. Y. Son, G. Lee, H. Wang, S. Samson, Q. Wei, Y. Zhu, W. You, *Nat Commun.* **2022**, *13*, 2739.

[21] S. Abbate, G. Longhi, F. Lebon, E. Castiglioni, S. Superchi, L. Pisani, F. Fontana, F. Torricelli, T. Caronna, C. Villani, R. Sabia, M. Tommasini, A. Lucotti, D. Mendola, A. Mele, D. A. Lightner, *J. Phys. Chem. C* **2014**, *118*, 1682–1695

[22] R. Hussain, T. Jávorfi, G. Siligardi, *Front. Chem.* **2021**, *9*, 616928.

[23] J. Bertrandie, J. Han, C. De Castro, E. Yengel, J. Gorenflot, T. Anthopoulos, F. Laquai, A. Sharma, D. Baran, *Adv. Mater.* **2022**, *34*, e2202575.

[24] L. J. A. Koster, V. D. Mihailetchi, P. W. M. Blom, *Applied Physics Letters* **2006**, *88*, 052104.

[25] L. Ye, H. Hu, M. Ghasemi, T. Wang, B. A. Collins, J. -H. Kim, K. Jiang, J. H. Carpenter, H. Li, Z. Li, T. McAfee, J. Zhao, X. Chen, J. L. Y. Lai, T. Ma, J. -L.; Bredas, H. Yan, H. Ade, Nature *Mater* **2018**, *17*, 253–260.

[26] a) P. Josse, L. Favereau, C. Shen, S. Dabos-Seignon, P. Blanchard, C. Cabanetos, J. Crassous, *Chem. Eur. J.* **2017**, *23*, 6277–6281; b) B. Rice, L. M. LeBlanc, A. Otero-de-la-Roza, M. J. Fuchter, E. R. Johnson, J. Nelson, K. E. Jelfs, *Nanoscale* **2018**, *10*, 1865–1876.